

# Effect of self-healing in closing cracks from the sulfate attack in Portland, supersulfated and alkali-activated cement

*Efeito da autocicatrização no fechamento de fissuras decorrentes do ataque por sulfato em cimento Portland, supersulfatado e álcali ativado*

Priscila Ongaratto Trentin 

Caroline Angulski da Luz 

Ronaldo Alves de Medeiros-Junior 

## Abstract

**S**elf-healing consists of closing cracks and recovering the watertight properties of cement-based materials and can occur by hydration of the materials of the mixture (autogenous) or by materials added to the mixture for this purpose (autonomous). This study consists of the use of stimulated self-healing as a way of mitigating sulfate attack (sodium and magnesium), with the evaluation of the influence of crystalline admixture in this process. For that, cycles of sulfate attack and self-healing (by wetting and drying cycles in water) were performed, aiming to evaluate the behavior of mortars with three types of cement: Portland, supersulfated, and alkali-activated. The results showed that self-healing was not sufficient to close cracks due to sulfate attack. This behavior was associated with the hypothesis that the high calcium content of the crystalline admixture reacted with the sulfates and formed expansive products, increasing the attack rate.

**Keywords:** Sulfate attack. Portland cement. Supersulfated cement. Alkali-activated cement. Self-healing. Crystalline admixture.

## Resumo

*A autocicatrização consiste no fechamento de fissuras e recuperação da estanqueidade dos materiais à base de cimento e pode ocorrer por hidratação dos materiais da mistura (autógena) ou por materiais adicionados à mistura para esse fim (autônoma). Este estudo consiste na utilização de autocicatrização autógena estimulada como forma de atenuar o ataque por sulfatos (sódio e magnésio), com a avaliação da influência de adição cristalizante neste processo. Para isso, foram realizados ciclos de ataque sulfatado e autocicatrização (ciclos de molhagem e secagem), com o objetivo de avaliar o comportamento de argamassas com três tipos de cimento: Portland, supersulfatado e álcali ativado. Os resultados mostraram que a autocicatrização não foi suficiente para fechar trincas devido ao ataque por sulfatos. Esse comportamento foi associado à hipótese de que o alto teor de cálcio da adição cristalizante reagiu com os sulfatos e formou produtos expansivos, aumentando a taxa de ataque.*

**Palavras-chave:** Ataque por sulfatos. Cimento Portland. Cimento supersulfatado. Cimento álcali-ativado. Autocicatrização. Adição cristalizante.

<sup>1</sup>Priscila Ongaratto Trentin  
<sup>1</sup>Universidade Federal do Paraná  
Curitiba - PR - Brasil

<sup>2</sup>Caroline Angulski da Luz  
<sup>2</sup>Universidade Tecnológica Federal do  
Paraná  
Pato Branco - PR - Brasil

<sup>3</sup>Ronaldo Alves de Medeiros-  
Junior  
<sup>3</sup>Universidade Federal do Paraná  
Curitiba - PR - Brasil

Recebido em 11/06/23  
Aceito em 25/07/23

## Introduction

The construction industry contributes significantly to the development of society, being responsible for improving people's quality of life. Despite this, the construction industry is responsible for the generation of large amounts of waste and the emission of polluting gases (Assi *et al.*, 2020; Li *et al.*, 2022).

An example of this is Portland cement (PC). Cement is the main constituent of concrete structures. The production of 1 ton of Portland cement generates approximately 1 ton of CO<sub>2</sub> in the calcination process of the raw materials. Currently, the cement industries are responsible for releasing a content between 5 and 8% of all CO<sub>2</sub> emitted into the atmosphere (Wei; Cen, 2019). In emerging countries such as India, Russia, South Africa, and Brazil, the trend is for the demand for cement-based products to grow 2.5 times by 2050. Thus, cement manufacturing will account for approximately 12 to 23% of global CO<sub>2</sub> emissions (Taylor; Tam; Gielen, 2006). In 2019, 54.5 million tons of cement were sold in Brazil (SNIC, 2019).

Thus, it is essential to increase the service life of cementitious materials to reduce the demand for new structures, which also reduces the consumption of raw materials and the emission of polluting gases (De Rooij *et al.*, 2013). Also, the development of new materials has gained importance, focusing on the use of industrial by-products, to reduce the consumption of raw materials (Li *et al.*, 2022).

Supersulfated cement (SSC) is an example of a sustainable material. SSC is essentially made of blast furnace slag, a by-product of the manufacture of pig iron. SSC must have a content of granulated blast furnace slag greater than 75%, calcium sulfate between 5 and 20%, Portland cement from 0 to 5%, and between 0 and 5% of other materials (ECS, 2010).

Another cement alternative to Portland cement is alkali-activated cement (AAC). AAC is a clinker-free cement, produced from the activation of industrial by-products and which is already being used in many countries (Provis, 2018). AAC is a cement adaptable to the by-products available in each region, as it allows the use of a range of materials. It can be used in various parts of the world to promote sustainable civil construction development (Nedeljković; Li; Ye, 2018).

Sulfate attack is one of the many degradation processes that affect the durability of cementitious materials. Sulfate attack affects structures exposed to groundwater, seawater, industrial effluents, and soil with sulfate concentrations. The sulfate ions react with the cement hydration phases when in contact with the cement matrix, and form expansive phases. This process generates cracking, degradation, and reduction of mechanical strength (Elahi *et al.*, 2021; De Belie *et al.*, 2018).

Sulfate attack is related to durability problems of cement-based materials. Magnesium and sodium sulfates are considered the most aggressive, due to the formation of ettringite and gypsum. Also, MgSO<sub>4</sub> promotes the formation of hydrated magnesium silicate (M-S-H) from the attack of hydrated calcium silicate gel (C-S-H), which is primarily responsible for the mechanical strength of Portland cement-based materials (Elahi *et al.*, 2021; Huang *et al.*, 2021). The formation of these expansive phases is associated with the appearance of cracks.

Previous studies have found that Portland cement is not resistant to sodium and magnesium sulfate. On the other hand, supersulfated and alkali-activated cement has low resistance to magnesium sulfate (Beltrame *et al.*, 2020; Pinto *et al.*, 2020a, 2020b; Trentin *et al.*, 2023; Zhang *et al.*, 2022).

The treatments for closing cracks in cementitious materials can be done passively or actively. Passive treatments are applied to existing structures and have several limitations that make their application difficult, such as low weather resistance, sensitivity to moisture, and poor adhesion to concrete. On the other hand, active treatment techniques, called self-healing techniques, can be used in different conditions, regardless of the fissure position (Štukovnik; Bokan-Bosiljkov; Marinšek, 2020).

In recent years, the number of researches focused on the self-healing of cementitious materials has grown significantly. Self-healing is an efficient technique for closing cracks and recovering mechanical and watertight properties of structures (Danish; Mosaberpanah; Salim, 2020). Self-healing is called autogenous when it occurs by delayed hydration of cement grains or carbonation. Mineral, expansive or crystalline admixtures may be used to promote autogenous self-healing. In this case, the process is called enhanced autogenous self-healing. There is also autonomous self-healing when the cement matrix receives specific materials to promote self-healing (Huang *et al.*, 2016).

Various materials can be added to the mixture to promote the self-healing process. According to Sahmaran, Yildirim and Erdem (2013), materials such as fly ash, silica fume, blast furnace slag, or clay act in the pozzolanic reaction, improving the matrix's self-healing potential. The inclusion of pozzolans can ensure the

self-healing of structures over a long time, even when repeated damage occurs. However, the pozzolanic reaction is dependent on the availability of calcium hydroxide in the system (Huang; Ye; Damidot, 2014).

Expansive agents and crystalline admixtures are also being used in cementitious matrices to promote stimulated autogenous self-healing, restoring water tightness and mechanical strength properties (Kanellopoulos; Qureshi; Al-Tabbaa, 2015; Reddy; Ramesh Macrin, 2020).

According to Sisomphon, Copuroglu and Koenders (2013), the wetting and drying cycles represent the best condition for the development of self-healing. The evaporation of excess water during the drying phase leads to an increase in the concentration of ions in the cracks, which promotes the development of chemical reactions and the precipitation of hydrated products. Furthermore, the penetration of CO<sub>2</sub> into the cracks during the drying period favors the formation of carbonates.

Furthermore, authors such as Ahn and Kishi (2010), Sisomphon, Copuroglu and Koenders (2012) and Munhoz *et al.* (2021), obtained satisfactory results of self-healing at 28 days. Thus, in order to accelerate the self-healing process of cracked mortars, wetting and drying cycles were carried out over a period of 28 days.

Thus, this study aimed to evaluate the self-healing potential of Portland cement, supersulfated cement, and alkali-activated cement mortars cracked by the expansive reaction of sulfate attack. No other study was found in the literature by these authors that investigated this relationship, reinforcing the innovation of this article.

## Experimental program

Figure 1 shows the composition of the mortars and the type of sulfate attack analyzed in each of them.

The sulfate attack was performed according to NBR 13583 (ABNT, 2014). Portland cement is not resistant to sodium sulfate or magnesium sulfate; therefore, this cement was evaluated in both attack conditions. Supersulfated and alkali-activated cements are resistant to Na<sub>2</sub>SO<sub>4</sub> attack (Beltrame *et al.*, 2020; Pinto *et al.*, 2020a, 2020b; Trentin *et al.*, 2023) and were evaluated only in the MgSO<sub>4</sub> attack.

## Materials

Ordinary Portland cement CEM I was used to comparing the results with SSC and AAC. Table 1 shows the chemical composition and other properties of the materials used.

The composition of the supersulfated cement used was 85.5: 9.5: 5, consisting of 85.5% blast furnace slag, 9.5% calcium sulfate, and 5% alkaline activator (CEM I). As verified by Trentin *et al.* (2023), the lower amount of calcium sulfate in the SSC composition reduces its resistance to magnesium sulfate attack, generating cracking of the specimens.

Figure 1 - Mortar composition and type of sulfate attack

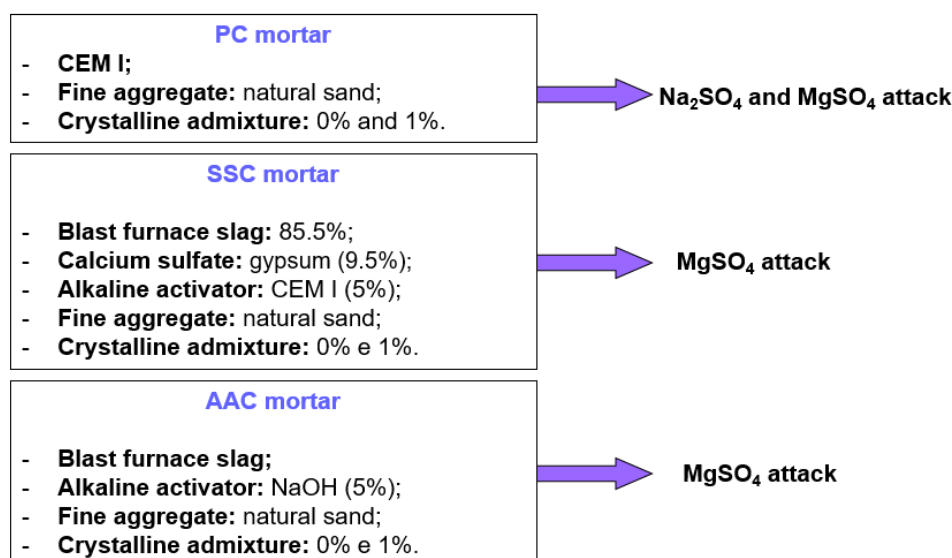


Table 1 - Chemical composition and other properties of the materials used

Elements	Percentage (%)				
	Slag (SSC)	Gypsum (SSC)	CEM I (SSC)	Slag (AAC)	Crystalline admixture
CaO	42.3	43.2	70.6	31.6	60.1
SiO <sub>2</sub>	39.0	0.3	12.0	40.5	8.6
Al <sub>2</sub> O <sub>3</sub>	8.7	-	3.8	14.3	2.6
MgO	5.5	0.1	0.5	7.5	2.2
MnO	1.5	-	-	1.2	-
SO <sub>3</sub>	0.9	55.0	8.6	0.1	6.5
Fe <sub>2</sub> O <sub>3</sub>	0.6	0.1	3.1	1.8	2.8
TiO <sub>2</sub>	0.6	-	-	1.0	-
K <sub>2</sub> O	0.5	< 0.1	1.3	0.9	1.1
SrO	0.2	0.1	-	0.1	-
BaO	0.1	-	-	0.1	-
Na <sub>2</sub> O	0.1	-	0.3	0.2	0.2
ZrO <sub>2</sub>	< 0.1	-	-	0.1	-
Y <sub>2</sub> O <sub>3</sub>	< 0.1	-	-	-	-
P <sub>2</sub> O <sub>5</sub>	< 0.1	< 0.1	-	< 0.1	-
Free CaO	-	-	-	-	-
Insoluble residue	-	-	-	-	-
Loss on ignition	0.41	0.97	-	0.7	16
CaO+MgO+SiO <sub>2</sub>	86.8	-	-	-	-
(CaO+MgO)/SiO <sub>2</sub>	1.23	-	-	-	-
Specific mass (g/cm <sup>3</sup> )	2.76	-	3.09	2.86	1.45
Specific surface (Blaine) (cm <sup>2</sup> /g)	-	-	4405	-	4991

The blast furnace slag, generated in coal furnaces, underwent a drying process in an oven, at a temperature of  $(105 \pm 2)$  °C, for 24 hours, and then it was ground for 3 hours. Figure 2 shows the analysis of X-ray diffraction (XRD), where the amorphism of the material was verified.

According to the EN 15743 (ECS, 2010) standard, the sum of CaO+MgO+SiO<sub>2</sub> must be greater than or equal to 66.7 and the CaO+MgO/SiO<sub>2</sub> ratio must be greater than or equal to 1 so that the slag can be used in the production of supersulfated cement. Thus, the slag used in this study complies with EN 15743 (ECS, 2010) (Table 1). Also, calcium sulfate (gypsum) was sieved through a 150 µm sieve and calcined at 650 °C for one hour at a heating rate of 50 °C/min. Portland cement (CEM I) was used as an alkaline activator in SSC mortars.

Alkali-activated cement was produced with blast furnace slag generated in a charcoal furnace, and activated with sodium hydroxide, according to Beltrame *et al.* (2020). The slag for AAC was dried in an oven at  $(105 \pm 2)$  °C for 24 hours and then ground for 2 hours. Figure 2(b) shows X-ray diffraction (XRD) analysis.

The alkaline activator for the production of alkali-activated cement was sodium hydroxide (NaOH), at a content of 5% in relation to the slag mass, as indicated by Langaro *et al.* (2020).

Normal sand was used in the production of mortars, according to NBR 7214 (ABNT, 2015). The granulometric fractions used were coarse (n° 16), medium coarse (n° 30), medium fine (n° 50), and fine (n° 100), in equal proportions. The specific gravity of the sand, determined according to the pycnometer method, was 1.93 g/cm<sup>3</sup>.

Crystalline admixture (Table 1) was used to assist in the self-healing process of the mortar specimens. The crystalline admixture acts on waterproofing by integral crystallization, being added to the mortar trace at the time of its production.

According to the manufacturer, the content of 0.8% in relation to the cement mass is indicated. The crystalline admixture content adopted in this study was 1%, as indicated by Munhoz *et al.* (2021) and Dobrovolski *et al.* (2021). XRD analyses of the anhydrous crystalline admixture (Figure 3(a)) and XRD and thermal analyses of the hydrated crystalline admixture (Figures 3(b) and 4) were performed. According to Figures 3 and 4, the crystalline admixture used is similar to Portland cement, with the same hydrated products identified.

Figure 2 - XRD analysis of (a) SSC slag and (b) AAC slag

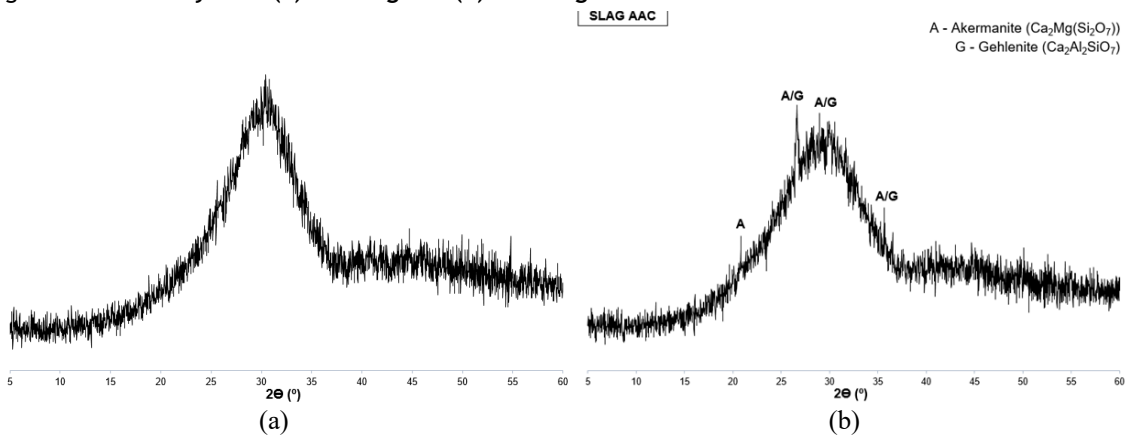


Figure 3 - XRD of (a) anhydrous crystalline admixture and (b) crystalline admixture paste

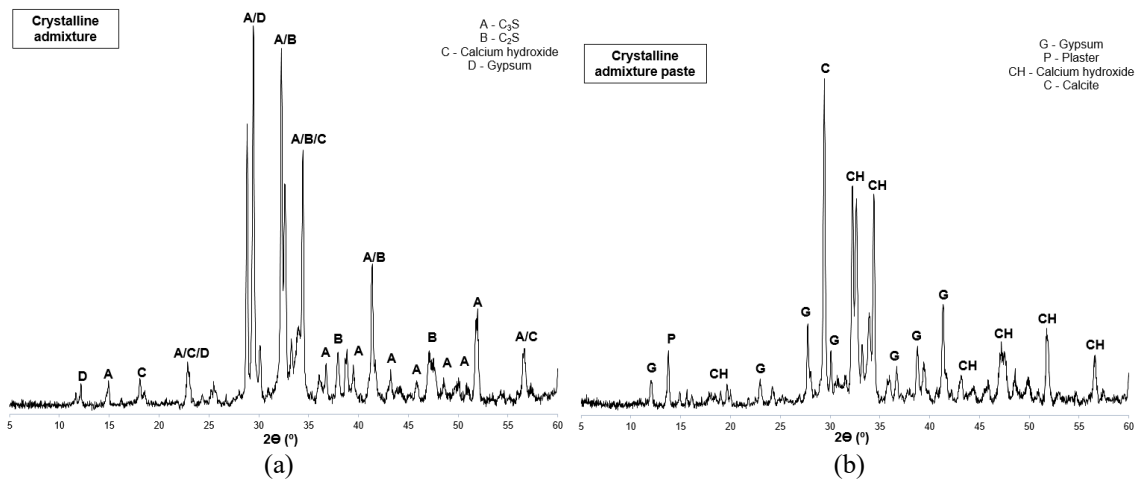
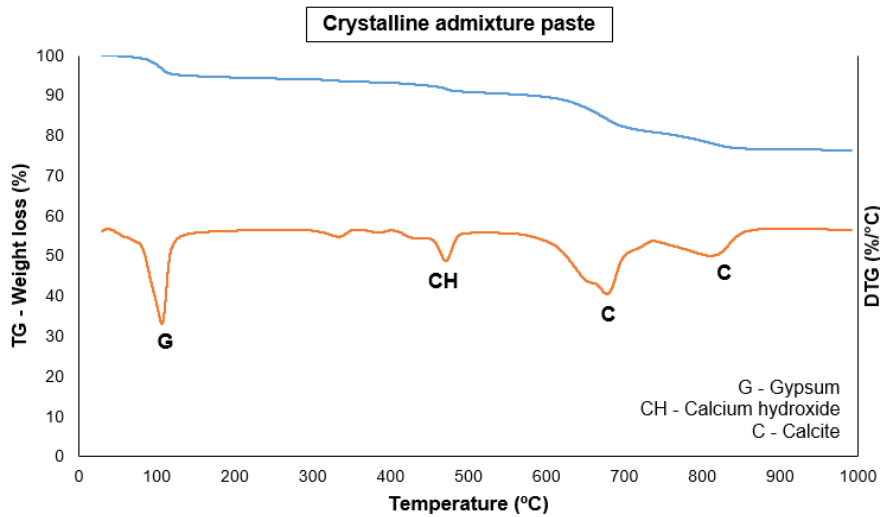


Figure 4 - Thermal analysis of the crystalline admixture paste



## Methods

Figure 5 shows the testing methodology developed in this study. The mix used to produce the mortars was 1: 3.2: 0.6 (cement: sand: water), with four specimens measuring 2.5 x 2.5 x 28.5 cm per mix. Table 2 shows the mortar mixture proportions, considering 100 g of cement in each composition.

The PC was demolded after 2 days. For SSC and AAC, more time was needed to allow demolding, 4 and 7 days, respectively. After demolding, the specimens were immersed in a solution of lime-saturated water and placed in a chamber, at a temperature of  $(23 \pm 2)$  °C, until the 14 days of age were completed. Then, the sulfate attack was started, with concentration of 10%, in an oven at a temperature of  $(40 \pm 2)$  °C, until the test specimens cracked, and the age varied according to the tested mortar mixture. The criterion for starting the self-healing cycles was determined by visualizing the cracks, with a crack opening limitation of 0.2 mm (200  $\mu$ m). The crack opening was measured with a fissure ruler at the location of the greatest width of the crack.

The crack opening limit was established according to the literature. Autogenous self-healing of concrete is only efficient for small cracks, with closure of up to 0.20 mm wide (BSI, 1987).

Wetting and drying cycles in water were performed to accelerate the self-healing mechanism. These cycles were applied after the mortars cracked in the sulfate attack. Four 7-day cycles were applied, with 3 days submerged in water and 4 air dry days, always in a chamber, at a temperature of  $(23 \pm 2)$  °C, according to the methodology proposed by Sisomphon, Copuroglu and Koenders (2013), Esteves, Trentin and Medeiros-Junior (2021) and Munhoz *et al.* (2021).

Test times for each type of cement are shown in Table 3. After the self-healing cycles, the specimens returned to the sulfate attack condition.

For the wetting and drying cycles, potable water was used, whose chemical analysis is shown in Table 4.

### Length and mass change tests

Weekly, the specimens were removed from the etching solution and had their surfaces dried to remove surface water. Subsequently, they were photographed and weighed and their dimensions were verified on a length dial indicator, with 0.001 mm accuracy.

### Immersion water absorption

The immersion water absorption test was performed according to Munhoz *et al.* (2021) and Dobrovolski *et al.* (2021), during the wetting and drying cycles. Four wetting and drying cycles of were performed lasting 7 days each. There were 4 days of exposure to air, when the dry weight was determined, and 3 days of immersion in water, when was determined the saturated weight.

Figure 5 - Sulfate attack and self-healing cycles

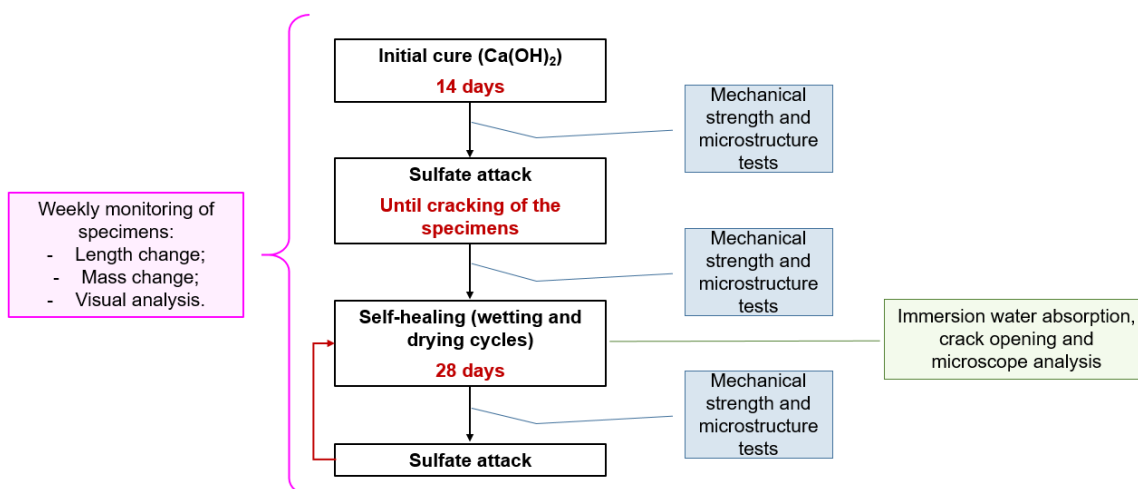


Table 2 - Mortar composition

Mix	Portland cement	Slag SSC	Slag AAC	Calcium sulfate	Alkaline activator	Crystalline admixture	Sand	Water
PC	100 g	-		-	-	-	320 g	60 g
PC+A	100 g	-		-	-	1 g	320 g	60 g
SSC	-	85.5 g		9.5 g	5 g (PC)	-	320 g	60 g
SSC+A	-	85.5 g		9.5 g	5 g (PC)	1 g	320 g	60 g
AAC	-	-	100 g	-	5 g (NaOH)	-	320 g	60 g
AAC+A	-	-	100 g	-	5 g (NaOH)	1 g	320 g	60 g

Table 3 - Analysis periods (time of each step)

Mix	Attack solution	Inicial cure	Sulfate attack	Age for onset of self-healing	Self-healing cycles	Sulfate attack	Test completion age
PC	Na <sub>2</sub> SO <sub>4</sub>	14 days	98 days	112 days	28 days	147 days	287 days
PC+A							
PC	MgSO <sub>4</sub>	14 days	252 days	-	-	-	266 days
PC+A							
SSC	MgSO <sub>4</sub>	14 days	49 days	63 days	28 days	91 days	182 days
SSC+A							
AAC	MgSO <sub>4</sub>	14 days	35 days	49 days	28 days	77 days	154 days
AAC+A							

Table 4 - Chemical analysis of potable water

Parameters	Average of the last 30 results	Minimum/Maximum Allowed	Unit
Color	2.0	15.0	uH-Un.Cor
Fluorides	0.7	0.6 to 1.1	mg/L F
Turbidity	1.0	5.0	NTU
pH	7.0	-	-
Chlorine Residue	1.0	0.2 to 5.0	mg/L Cl
Aluminum	0.1	0.2	mg/L Al
Iron	0.0	0.3	mg/L Fe
Manganese	0.0	0.1	mg/L Mn
Microcystins	-	1.0	ug/L
Total coliforms	0.0	0.0	NMP/100mL
Escherichia Coli	0.0	0.0	NMP/100mL

### Mechanical resistance

Flexural tensile strength and compressive strength tests were performed. Prismatic specimens measuring 4 x 4 x 16 cm were used with the same mortar mixtures and under the same conditions of attack by sulfates.

The mechanical strength analyzes were performed at the age of 14 days, the age of start sulfate attack, the start date of self-healing cycles, and at the end of 28 days of self-healing cycles, with age varying according to the mortar mix since the appearance of cracks varied according to the type of cement investigated.

### Crack mapping

Macro and mesoscale analyzes were used to monitor the evolution of self-healing. Prismatic specimens (2.5 x 2.5 x 28.5) cm were used to monitor the evolution of cracks and their self-healing. The macroscale monitoring was done through photos of the specimens on the measurement dates of length and mass change. Mesoscale analyzes were performed with a digital microscope (with up to 1000x magnification), during the wetting and drying cycles, with monitoring of crack opening sizes, with a calculation of the average crack opening for each mortar mix.

XRD (X-ray Diffractometry) and TG/DTG (Thermogravimetry and Derived Thermogravimetry) analyzes were performed for microstructural monitoring, at the same ages defined for mechanical strength. The paste samples were milled until they passed through a 150  $\mu\text{m}$  sieve.

The XRD analyses were performed under the following conditions: wavelength of 1.54  $\text{\AA}$ , over a range from 5° to 60° (2 $\theta$ ), scanning speed of 3°/min, and Cu-K $\alpha$  radiation, 40 kV/30 mA. Thermal analysis tests were performed in SDT Q-600 equipment, under the following conditions: sample mass of 10 mg, heating range from 30 °C to 1000 °C, a heating rate of 10 °C/min, a nitrogen atmosphere, and gas flow of 100 ml/min.

## Results and discussions

### Portland cement: sodium sulfate attack

Figures 6(a) and 7(a) show length and mass change in Portland cement under the Na<sub>2</sub>SO<sub>4</sub> attack. The dotted vertical lines indicate the period of self-healing cycles.

According to Figure 6(a), the PC specimens initially showed a shrinkage trend. From 182 days onwards, there was an expansion of the samples, with a maximum value close to 0.3% at 252 days. PC+A, on the other hand, showed a tendency to expand throughout the test, with a maximum expansion of 0.72% at 301 days. Regarding mass change, PC and PC+A showed a tendency to gain mass, reaching 6.5% for PC and 10% for PC+A.

The expansion combined with the increase in mass indicates the formation of expansive phases due to the Na<sub>2</sub>SO<sub>4</sub> attack. Similar results were obtained by Pinto *et al.* (2020a), who also evaluated sodium sulfate attack on Portland cement according to NBR 13583 (ABNT, 2014), and verified the expansion trend after 120 days of the attack, as well as a mass gain close to 1% in the same period. The low resistance of PC is associated with the greater availability of aluminates and portlandite, represented by the high content of C<sub>3</sub>A and the high content of clinker, respectively, in this cement. These compounds tend to react with sodium sulfate, forming gypsum and ettringite.

This hypothesis is confirmed in the microstructural analyzes of XRD and TG/DTG (Figures 8 and 9), where a reduction in the intensity of calcium hydroxide peaks was observed during the sulfate attack process, which indicates the consumption of products hydrated by the attack, with the formation of ettringite, characteristic product of the sodium sulfate attack. In the microstructure analysis of the PC+A, an increase in the intensity of the ettringite peaks over time was also observed. Despite this, there was maintenance in the intensity of the peaks of hydrated phases formed, with an increase in the intensity of the peaks of calcium hydroxide during the 28 days of the self-healing cycle (119 to 147 days). This result shows the effect of the crystalline admixture on the cement matrix.

Figure 6 - Length change of (a) PC - Na<sub>2</sub>SO<sub>4</sub>, (b) PC - MgSO<sub>4</sub>, (c) SSC - MgSO<sub>4</sub> and (d) AAC - MgSO<sub>4</sub>

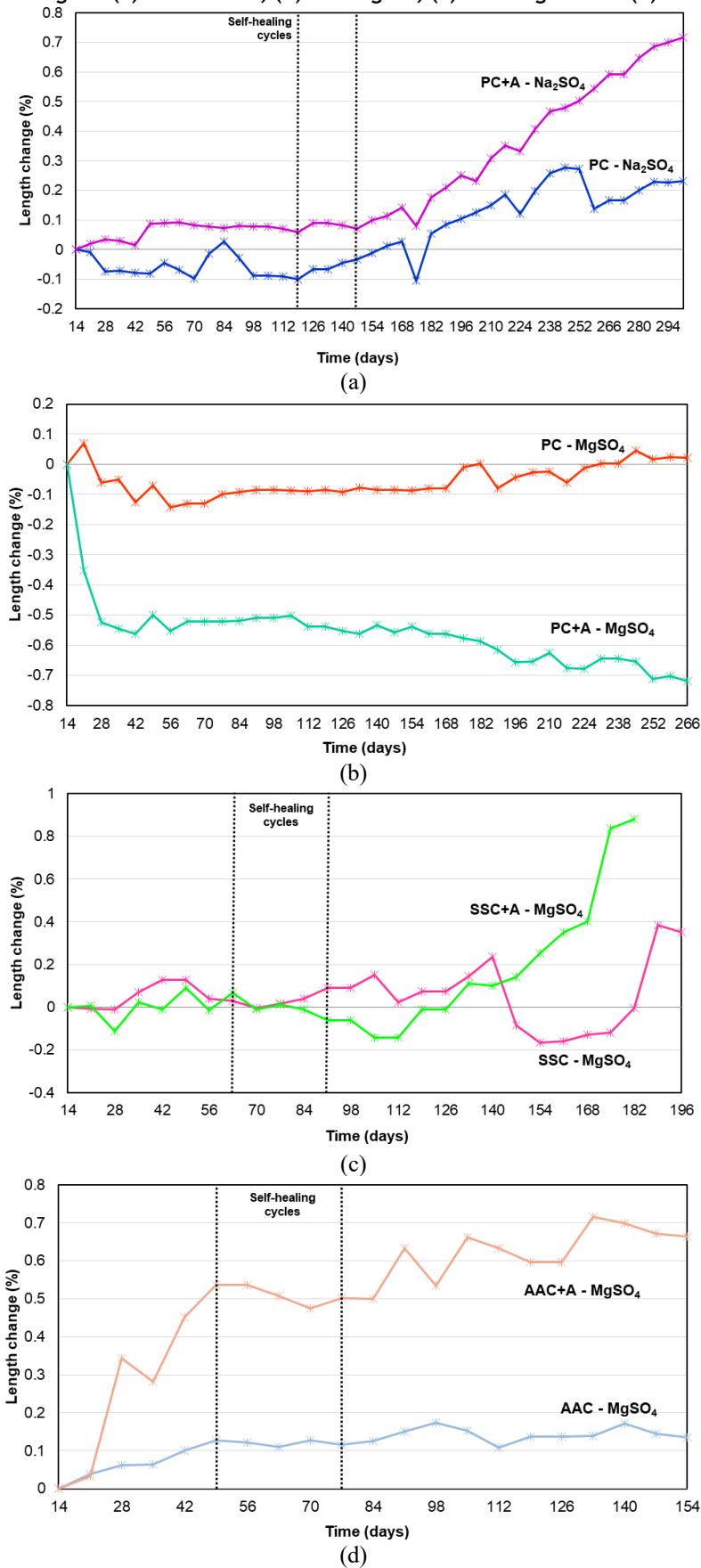


Figure 7 - Mass change of (a) PC - Na<sub>2</sub>SO<sub>4</sub>, (b) PC - MgSO<sub>4</sub>, (c) SSC - MgSO<sub>4</sub> and (d) AAC - MgSO<sub>4</sub>

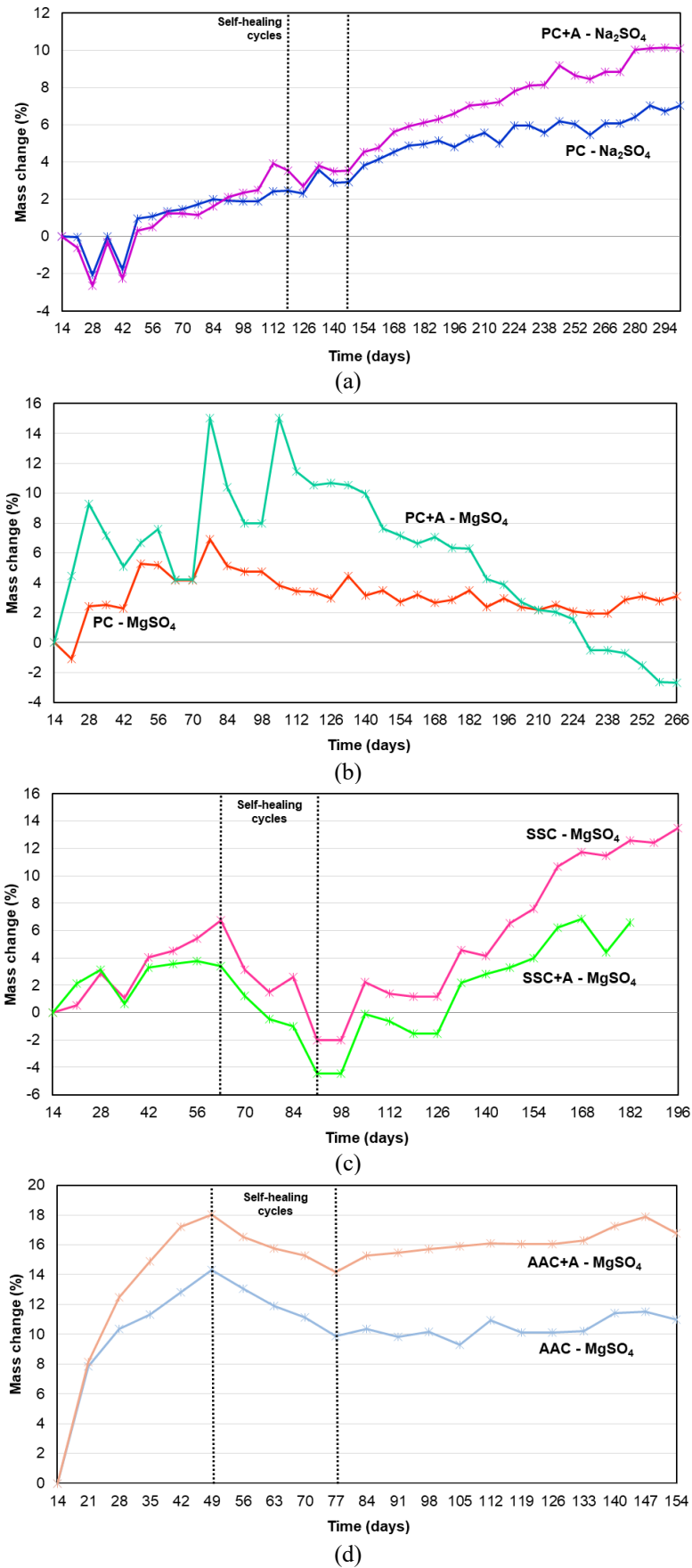
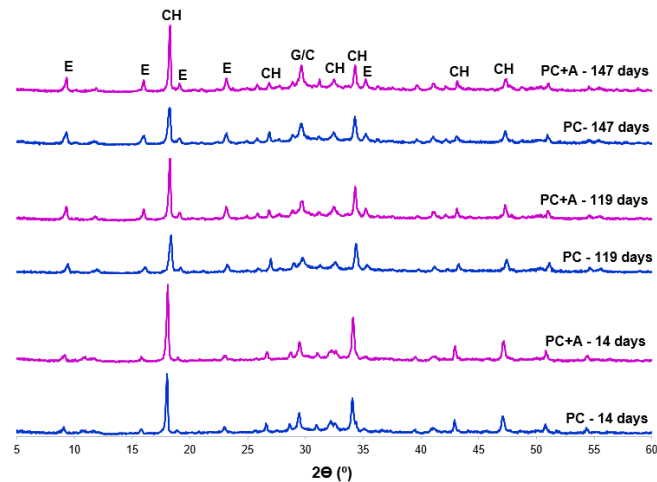
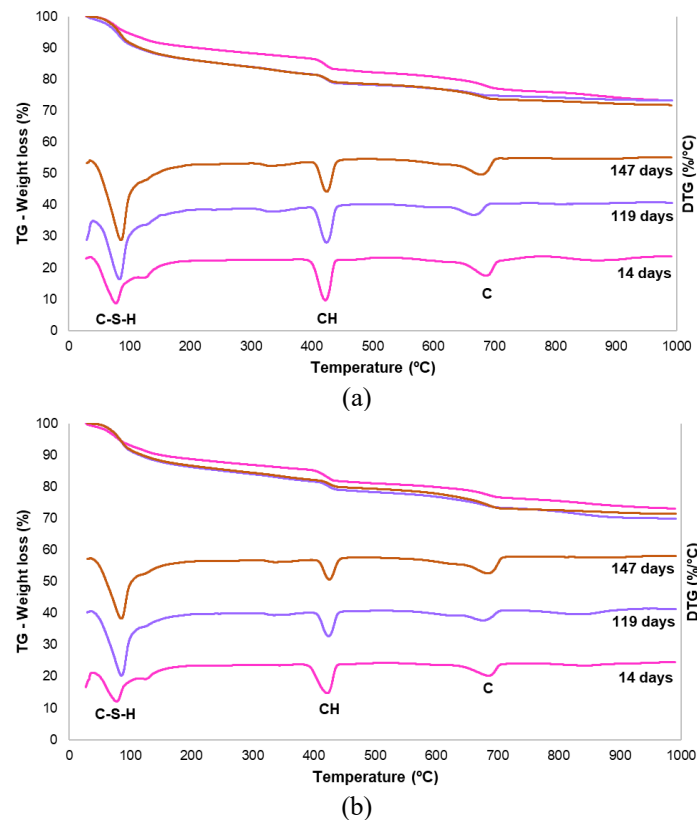


Figure 8 - XRD of PC - Na<sub>2</sub>SO<sub>4</sub>

Note: C: calcite; CH: calcium hydroxide; E: ettringite; and G: gypsum.

Figure 9 - TG/DTG of PC in Na<sub>2</sub>SO<sub>4</sub> (a) CP and (b) CP+A

Note: C-S-H: hydrated calcium silicate; CH: calcium hydroxide; and C: calcite.

These results are supported by the compressive strength test (Figure 10). The compressive strength results also showed the action of the crystalline admixture, with an increase in compressive strength over time.

In the PC in Na<sub>2</sub>SO<sub>4</sub> attack, the crack formation was observed after 119 days (105 days of sulfate attack). Figure 11 (a and b) show the microscope images at the beginning of the self-healing process. Small cracks were formed at the ends of the mortar specimens with an average size between 0.03 and 0.05 mm.

At the end of the wetting and drying cycles, the average size of the cracks varied between 0.03 and 0.07 mm (Figure 11(c) and (d)). Thus, there was no self-healing of the cracks during the 28 days of wetting and drying

cycles. This increase in the crack opening provided an increase in the immersion water absorption of the mortars (Figure 12(a)).

The main justification for the absence of self-healing in this condition is related to the high aggressiveness of the sulfate attack since it is a continuous degradation mechanism. Even after removing the specimens from the sulfate solution, for the execution of the wetting and drying cycles in water, part of the sulfates remained inside the mortars, continuing the attack. Thus, the contribution of self-healing was insufficient to mitigate the attack by sodium sulfate under the conditions selected in this study using Portland cement.

Figure 10 - Compressive strength of (a) PC -  $\text{Na}_2\text{SO}_4$ , (b) SSC -  $\text{MgSO}_4$  and (c) AAC -  $\text{MgSO}_4$

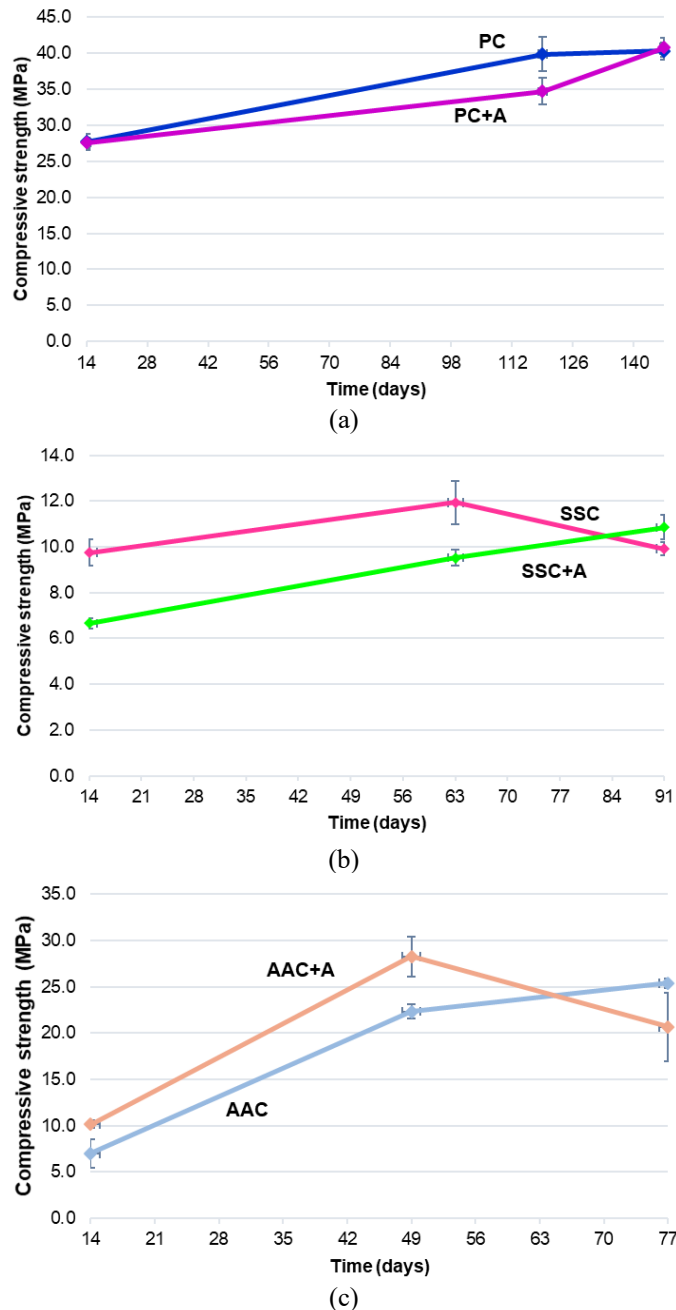
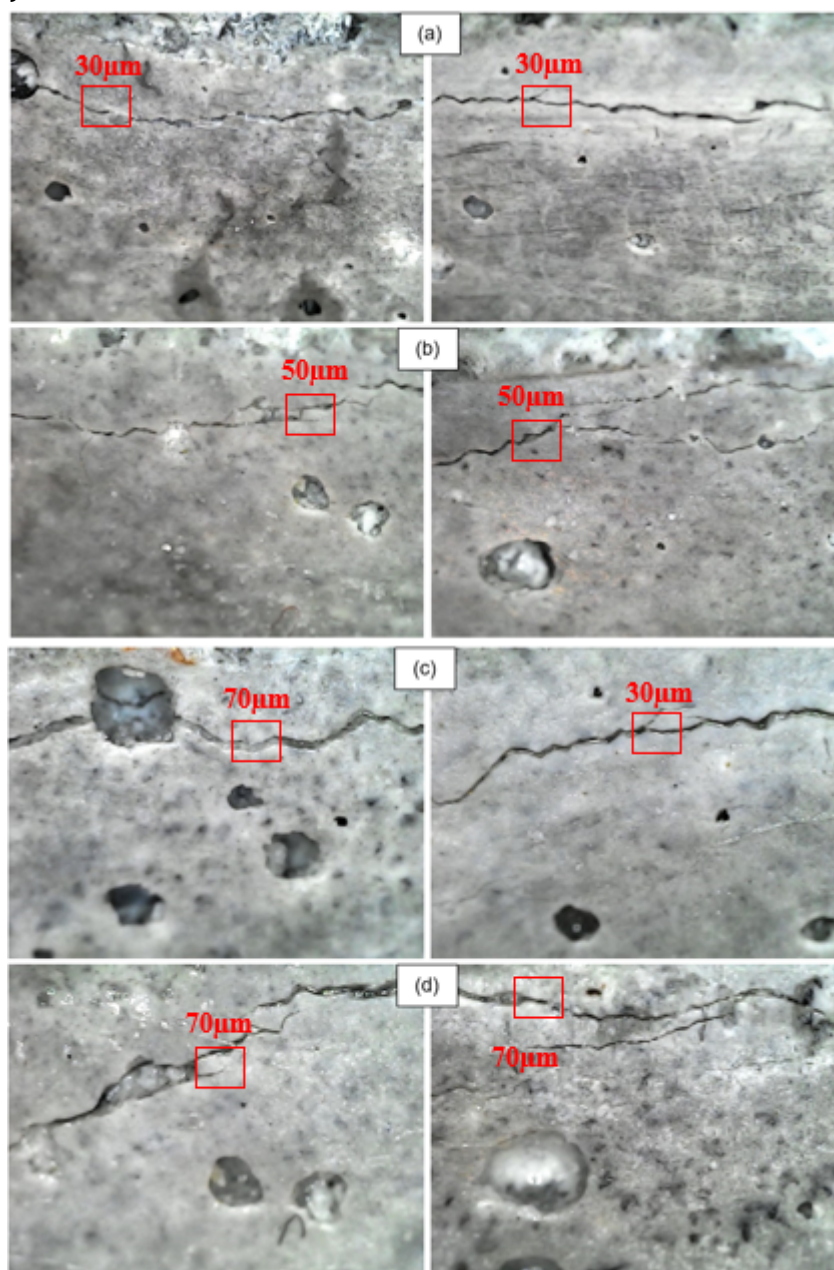


Figure 11 - PC mortar matrix at  $\text{Na}_2\text{SO}_4$  (a) PC - 119 days, (b) PC+A - 119 days, (c) PC - 147 days and (d) PC+A - 147 days



### Portland cement: magnesium sulfate attack

Figures 6(b) and 7(b) show length and mass change in Portland cement under the  $\text{MgSO}_4$  attack. In the  $\text{MgSO}_4$  attack, a similar behavior to the attack by  $\text{Na}_2\text{SO}_4$  was observed, with a shrinkage of 0.1%. However, for PC+A, a remarkable shrinkage of the specimens was observed, with values greater than 0.7% in 266 days of analysis.

The shrinkage of PC+A samples may be associated with the greater availability of calcium in this system, due to the crystalline admixture, rich in calcium (Table 1). As magnesium sulfate consumes calcium to form expansive phases such as ettringite, gypsum, and brucite, the greater availability of calcium may have fostered the attack process, resulting in the bending of the specimens, as evidenced by the length change.

Regarding the mass change, PC and PC+A showed mass gain initially, as the most expressive values for PC+A, greater than 15% at 105 days. This behavior is related to the formation of a white surface layer on the

specimens (Figure 13), as well as the suspension of this material in solution, from the age of 21 days (after 7 days of attack by  $\text{MgSO}_4$ ). From 210 days, in the PC+A specimens, the mass reduction was observed, due to the degradation of the samples.

Figure 12 - Immersion water absorption during self-healing cycles for (a) PC in  $\text{Na}_2\text{SO}_4$ , (b) SSC in  $\text{MgSO}_4$  and (c) AAC in  $\text{MgSO}_4$

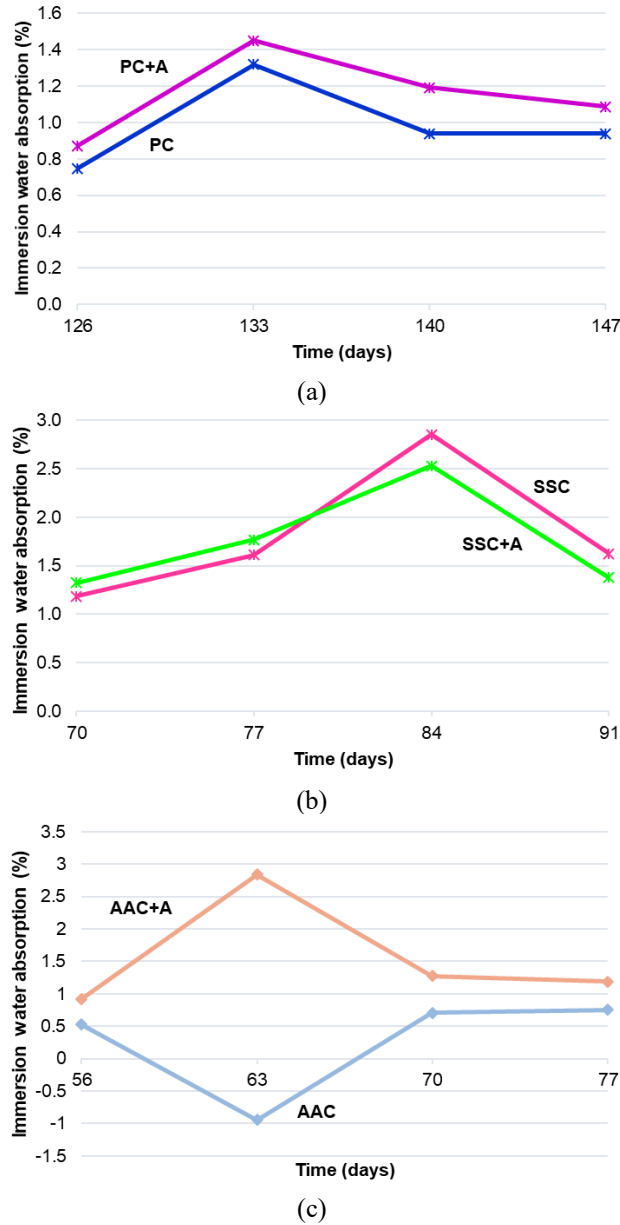
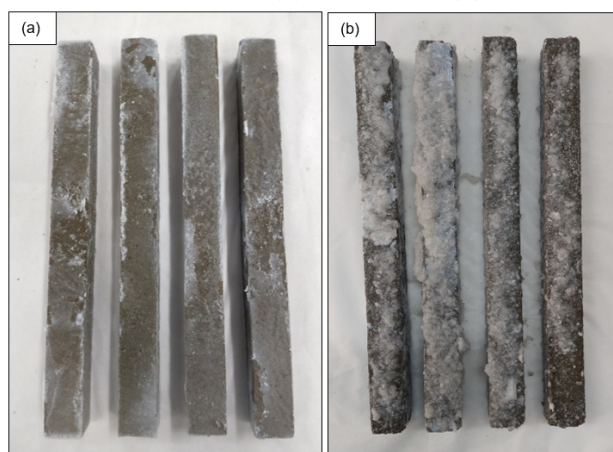


Figure 13 - PC+A mortars under  $MgSO_4$  attack at (a) 21 days and (b) 77 days

Microstructural analyzes of XRD and TG/DTG were used to identify the white material formed. According to Figures 14 and 15, gypsum was identified. However, due to the formation of gypsum on the surface of the specimens, it was not possible to observe the formation of cracks in this case even after 266 days of testing. Therefore, the self-healing step (wetting and drying cycles) was not performed in these samples, due to the absence of cracks in the mortars.

### Supersulfated cement: magnesium sulfate attack

Figures 6(c) and 7(c) show the length and mass change in SSC mortars in a magnesium sulfate solution. The dotted vertical lines indicate the period of self-healing cycles. Similar behavior was observed for the two mortars (SSC and SSC+A) up to 140 days, with alternation between shrinkage and expansion, not exceeding 0.2%, in agreement with Pinto *et al.* (2020b), who evaluated the behavior of SSC exposed to  $MgSO_4$  for 140 days. From 140 days, however, there was a trend of shrinkage in SSC (up to 175 days) and significant expansion for SSC+A mortars, exceeding 0.8% expansion.

Regarding mass change, a similar behavior was observed for the two mortar mixtures, with mass increase until the start date of the self-healing cycles. During the self-healing cycles (63 to 91 days) there was a tendency for mass loss (with percentages up to 5%). Upon returning to the sulfate attack, SSC and SSC+A again showed a mass increase. This shows that, despite the degradation of the specimens, which resulted in mass loss, the generation of expansive phases by the sulfate attack is more expressive, causing again the mass gain. An expressive mass increase was also observed by Pinto *et al.* (2020b) with percentages reaching 12%.

The behavior of length and mass change is justified in the XRD and TG/DTG analyses (Figures 16 and 17). The SSC pastes showed an increase in the intensity of gypsum formation until 63 days, the start date of the cycles of self-healing, which demonstrates the aggressiveness of the magnesium sulfate attack, whose main phase formed in SSC is gypsum.

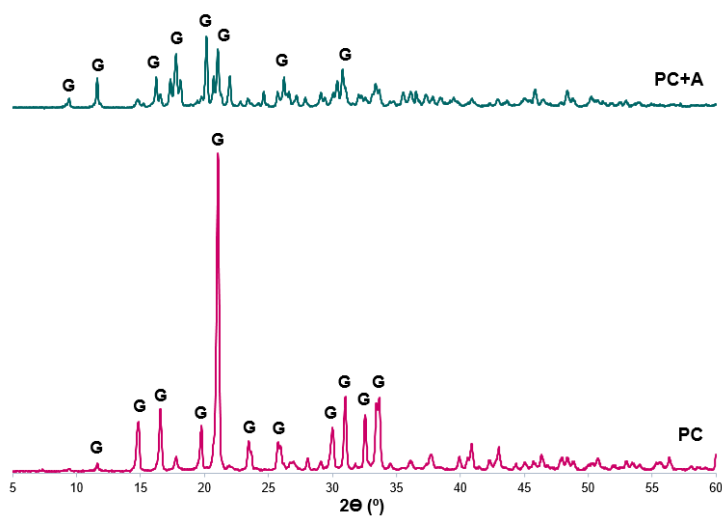
The greater expansion and mass increase of the SSC+A, in addition to the increase in the intensity of phase peaks over time, justify the continuous increase in compressive strength of this mortar, as the formation of expansive phases initially densifies the cementitious matrix, which generates an increase in mechanical strength (Figure 10(b)). The microstructural analyzes (Figures 16 and 17) supports the reduction in the mechanical strength of the SSC during the self-healing cycles, as a reduction in the phases formed was noted.

The supersulfated cement showed cracking at 63 days of age, after only 49 days of sulfate attack. These results may be associated with the low strength of this material (less than 10 MPa). Figure 18 show the microscopic analyzes at the beginning and end of the self-healing cycles, at 63 and 91 days, respectively.

In SSC, the aggressiveness of the attack did not allow self-healing of fissures. There was an increase in the opening of cracks, with breakage of cracks during the self-healing cycles, which did not allow monitoring of the same cracks during this period.

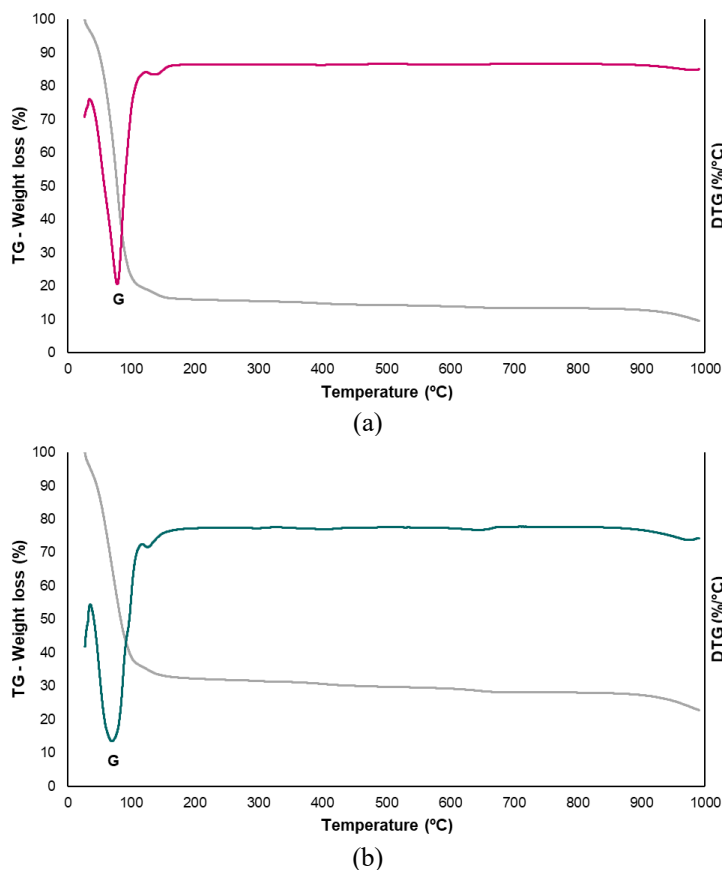
The increase in crack opening shows the aggressiveness of magnesium sulfate attack and the absence of self-healing, as observed in the water absorption test (Figure 12(b)). At 182 and 196 days, all the SSC+A and SSC specimens ruptured.

Figure 14 - XRD of formed material in PC on MgSO<sub>4</sub> attack

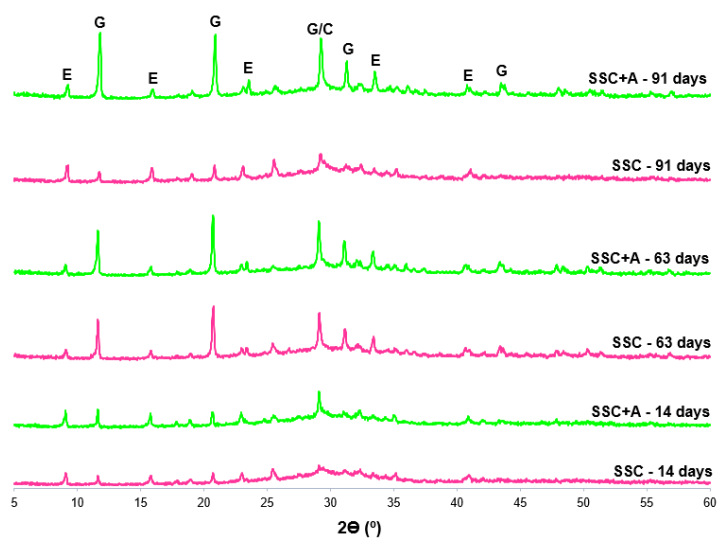


Note: G: gypsum.

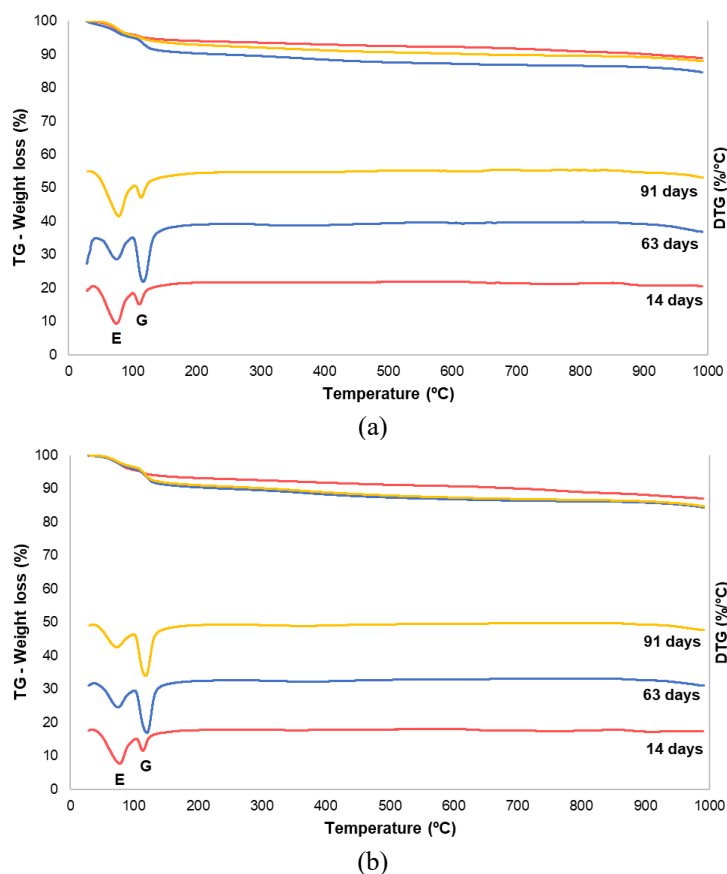
Figure 15 - TG/DTG of formed material in PC on MgSO<sub>4</sub> attack of (a) PC and (b) PC+A



Note: G: gypsum.

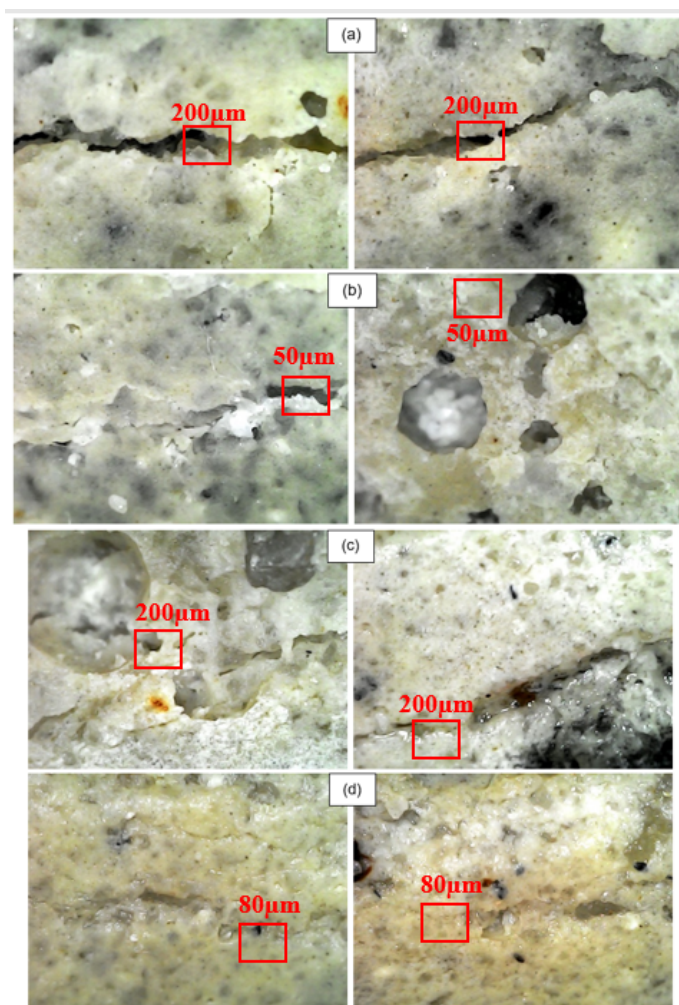
Figure 16 - XRD of SSC -  $MgSO_4$ 

Note: C: calcite; E: ettringite; and G: gypsum.

Figure 17 - TG/DTG of SSC in  $MgSO_4$  (a) SSC and (b) SSC+A

Note: E: ettringite; and G: gypsum.

Figure 18 - SSC mortar matrix in  $MgSO_4$  (a) SSC - 63 days, (b) SSC+A - 63 days, (c) SSC - 91 days and (d) SSC+A - 91 days



### Alkali-activated cement: magnesium sulfate attack

Figures 6(d) and 7(d) show the length and mass change in AAC mortars in a magnesium sulfate solution. The dotted vertical lines indicate the period of self-healing cycles. Expansive behavior was observed for AAC+A. In the AAC, there was no remarkable length change. Thus, the crystalline admixture may be promoting the magnesium sulfate attack process and the consequent formation of expansive phases, mainly due to the high calcium content in its chemical composition (Table 1).

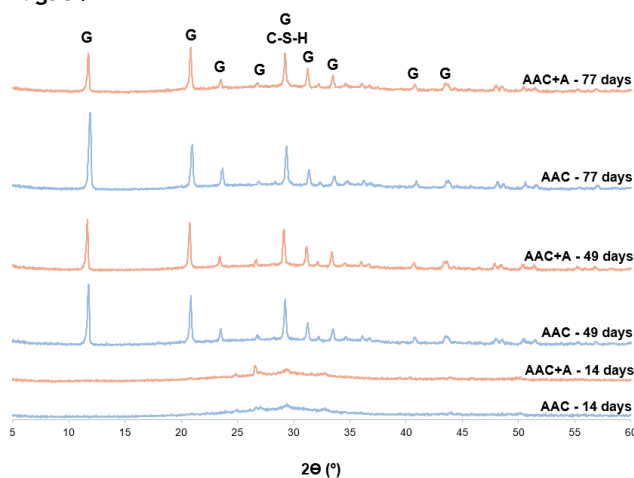
A significant mass increase was observed for AAC and AAC+A. AAC+A showed a mass gain of 18% at 49 days of age (28 days of  $MgSO_4$  attack). The mass change results followed the trend observed by Beltrame *et al.* (2020), but more expressively. However, as the authors evaluated the attack by sulfate in different methodologies and using specimens of paste, which has lower permeability to sulfates, the results found are consistent with what was expected for this type of cement.

The XRD analysis (Figure 19) supports the expressive mass gain results. Intense gypsum formation was observed at 49 and 77 days, the start and end dates of the self-healing cycles, respectively. Also, according to Figure 10(c), despite the aggressiveness of the attack, the AAC showed an increase in resistance over time. The AAC+A showed a reduction in mechanical strength during the self-healing cycles.

The mechanical strength of the alkali-activated cement at 14 days was lower than that obtained by Beltrame *et al.* (2020), who obtained values greater than 30 MPa. In this study, the average compressive strength at the start of sulfate attack was only 7 MPa, which justifies the early degradation of the samples, which showed crack formation at 49 days. However, unlike SSC, the strength of AAC increased significantly over time,

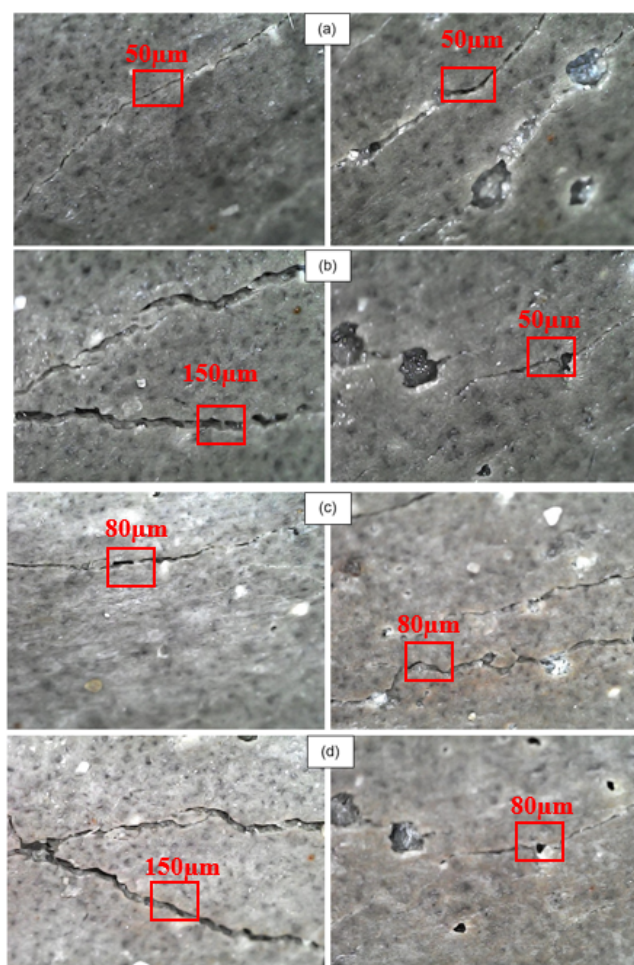
surpassing the value of 20 MPa after 42 days (Figure 10(c)). For the AAC, the self-healing cycles were performed between 49 and 77 days (Figure 20).

Figure 19 - XRD of AAC - MgSO<sub>4</sub>



Note: C-S-H: hydrated calcium silicate; and G: gypsum.

Figure 20 - AAC mortar matrix in MgSO<sub>4</sub> (a) AAC - 49 days, (b) AAC+A - 49 days, (c) AAC - 77 days and (d) AAC+A - 77 days



The alkali-activated cement with crystalline admixture (AAC+A) showed the largest crack openings, with values reaching 0.15 mm. In the AAC, the cracks had a maximum dimension of approximately 0.08 mm. In both cases, an increase in the crack opening was observed during the self-healing cycles. The immersion water absorption test also proved that there was no self-healing (Figure 12 (c)). The absorption at the end of the self-healing cycles was similar to that verified at the beginning.

## Conclusions

From the results obtained, the following conclusions are reached:

- (a) the low mechanical strength of SSC and AAC resulted in significant degradation of the mortar specimens at the beginning of the magnesium sulfate attack process. The low mechanical strength is related to the mortar mixture proposed by NBR 13583 (ABNT, 2014), which provides for the use of a water-to-cement ratio of 0.60. In addition, the low strength at early ages is also related to the compositions, materials, and activators used in the production of supersulfated and alkali-activated cements;
- (b) there was difficulty in identifying cracks during the magnesium sulfate attack on Portland cement due to the formation of gypsum on the surface of the specimens even the specimens showing marked expansion;
- (c) the use of the crystalline admixture indicated that this material did not contribute to the autogenous self-healing of the mortars due to the chemical composition of the material, with a high concentration of CaO (60.1%). Available calcium can react with sulfates to form expansive phases, increasing the attack rate; and
- (d) the 28 days of self-healing provided were not enough to seal the cracks in all the cements analyzed. Exposure of Portland cement to sodium sulfates, and the exposure of supersulfated and alkali-activated cements to magnesium sulfates caused cracks in the mortars. However, these cracks were not closed during self-healing. In some cases, there was an increase in the width of the cracks during the wetting and drying cycles, resulting in an increase in water absorption by immersion. Thus, further studies should improve the strength of supersulfated and activated alkali cements at an early age so that they can be subjected to sulfate attack. In addition, the time and conditions of self-healing must be modified so that the fissures can be self-healed.

## References

- AHN, T. H.; KISHI, T. Crack self-healing behavior of cementitious composites incorporating various mineral admixtures. **Journal of Advanced Concrete Technology**, v. 8, n. 2, p. 171-186, 2010.
- ASSI, L. N. *et al.* Review of availability of source materials for geopolymers/sustainable concrete. **Journal of Cleaner Production**, 263, 121477, 2020.
- ASSOCIAÇÃO BRASILEIRA DE NORMAS TÉCNICAS. **NBR 13583**: cimento Portland: determinação da variação dimensional de barras de argamassa de cimento Portland expostas à solução de sulfato de sódio. Rio de Janeiro, 2014.
- ASSOCIAÇÃO BRASILEIRA DE NORMAS TÉCNICAS. **NBR 7214**: areia normal para ensaio de cimento: especificação. Rio de Janeiro, 2015.
- BELTRAME, N. A. M. *et al.* Alkali activated cement made from blast furnace slag generated by charcoal: Resistance to attack by sodium and magnesium sulfates. **Construction and Building Materials**, v. 238, 117710, 2020.
- BRITISH STANDARDS INSTITUTION. **BS 8007**: code of practice for design of concrete structures for retaining aqueous liquids (Withdrawn). London, 1987.
- DANISH, A.; MOSABERPAHAH, M. A.; SALIM, M. U. Past and present techniques of self-healing in cementitious materials: A critical review on efficiency of implemented treatments. **Journal of Materials Research and Technology**, v. 9, n. 3, p. 6883-6899, 2020.
- DE BELIE, N. *et al.* A review of self-healing concrete for damage management of structures. **Advanced materials interfaces**, v. 5, n. 17, p. 1800074, 2018.

DE ROOIJ, M. *et al.* (ed.). **Self-healing phenomena in cement-based materials**: state-of-the-art report of RILEM technical committee 221-SHC: self-Healing phenomena in cement-Based materials. Berlin: Springer Science & Business Media, 2013.

DOBROVOLSKI, M. E. *et al.* Effect of crystalline admixture and polypropylene microfiber on the internal sulfate attack in Portland cement composites due to pyrite oxidation. **Construction and Building Materials**, v. 308, 125018, 2021.

ELAHI, M. M. A. *et al.* Improving the sulfate attack resistance of concrete by using supplementary cementitious materials (SCMs): a review. **Construction and Building Materials**, v. 281, 122628, 2021.

ESTEVEZ, I. C. A.; TRENTIN, P. O.; MEDEIROS-JUNIOR, R. A. Effect of fly ash contents in autogenous self-healing of conventional concretes analyzed using different test tools. **Journal of Materials in Civil Engineering**, v. 33, n. 7, p. 04021157, 2021.

EUROPEAN COMMITTEE FOR STANDARDIZATION. **EN 15743**: supersulfated cement: composition, specifications and conformity criteria. Berlin, 2010.

HUANG, H.; YE, G.; DAMIDOT, D. Effect of blast furnace slag on self-healing of microcracks in cementitious materials. **Cement and Concrete Research**, v. 60, p. 68-82, 2014.

HUANG, Q. *et al.* Will the magnesium sulfate attack of cement mortars always be inhibited by incorporating nanosilica? **Construction and Building Materials**, v. 305, 124695, 2021.

HUANG, H. *et al.* Self-healing in cementitious materials: materials, methods and service conditions. **Materials & Design**, v. 92, p. 499-511, 2016.

KANELLOPOULOS, A.; QURESHI, T. S.; AL-TABBAA, A. Glass encapsulated minerals for self-healing in cement based composites. **Construction and Building Materials**, v. 98, p. 780-791, 2015.

LANGARO, E. A. *et al.* Use of slag (GBFS) generated in charcoal blast furnace as raw material in alkali-activated cement. **Journal of Thermal Analysis and Calorimetry**, v. 142, n. 3, p. 1223-1231, 2020.

LI, X. *et al.* A systematic review of waste materials in cement-based composites for construction applications. **Journal of Building Engineering**, v. 45, 103447, 2022.

MUNHOZ, G. S. *et al.* Effect of improved autogenous mortar self-healing in the alkali-aggregate reaction. **Cement and Concrete Composites**, v. 117, 103905, 2021.

NEDELJKOVIĆ, M.; LI, Z.; YE, G. Setting, strength, and autogenous shrinkage of alkali-activated fly ash and slag pastes: effect of slag content. **Materials**, v. 11, n. 11, p. 2121, 2018.

PINTO, S. R. *et al.* Behavior of mortars exposed to attack by sodium and magnesium sulfate. **Journal of Building Pathology and Rehabilitation**, v. 5, n. 1, p. 1-7, 2020a.

PINTO, S. R. *et al.* Durability of phosphogypsum-based supersulfated cement mortar against external attack by sodium and magnesium sulfate. **Cement and Concrete Research**, v. 136, 106172, 2020b.

PROVIS, J. L. Alkali-activated materials. **Cement and Concrete Research**, v. 114, p. 40-48, 2018.

REDDY, C. M. K.; RAMESH, B.; MACRIN, D. Effect of crystalline admixtures, polymers and fibers on self healing concrete-a review. **Materials Today: Proceedings**, v. 33, p. 763-770, 2020.

SAHMARAN, M.; YILDIRIM, G.; ERDEM, T. K. Self-healing capability of cementitious composites incorporating different supplementary cementitious materials. **Cement and Concrete Composites**, v. 35, n. 1, p. 89-101, 2013.

SINDICATO NACIONAL DA INDÚSTRIA DO CIMENTO. **Consumo aparente de cimento por regiões e estados**. 2019. Available: <http://snic.org.br/numeros-industria.php>. Access: 7 abr. 2022.

SISOMPHON, K.; COPUROGLU, O.; KOENDERS, E. A. B. Effect of exposure conditions on self healing behavior of strain hardening cementitious composites incorporating various cementitious materials. **Construction and Building Materials**, v. 42, p. 217-224, 2013.

SISOMPHON, K.; COPUROGLU, O.; KOENDERS, E. A. B. Self-healing of surface cracks in mortars with expansive additive and crystalline additive. **Cement and Concrete Composites**, v. 34, n. 4, p. 566-574, 2012.

ŠTUKOVNIK, P.; BOKAN-BOSILJKOV, V.; MARINŠEK, M. ACR in dolomitic aggregate concrete for an autogenous self-healing process. **Materiali in Tehnologije**, v. 54, n. 3, p. 379-384, 2020.

TAYLOR, M.; TAM, C.; GIELEN, D. Energy efficiency and CO<sub>2</sub> emissions from the global cement industry. **Korea**, v. 50, n. 2/2, p. 61-67, 2006.

TRENTIN, P. O. *et al.* Influence of content and source of calcium sulfate on supersulfated cement exposed to sodium and magnesium sulfate attack at later ages. **Journal of Materials in Civil Engineering**, v. 35, n. 1, 04022364, 2023.

WEI, J.; CEN, K. Empirical assessing cement CO<sub>2</sub> emissions based on China's economic and social development during 2001–2030. **Science of the Total Environment**, v. 653, p. 200-211, 2019.

ZHANG, J. *et al.* Reaction mechanism of sulfate attack on alkali-activated slag/fly ash cements. **Construction and Building Materials**, v. 318, 126052, 2022.

#### **Priscila Ongaratto Trentin**

Conceptualization, Data curation, Formal analysis, Investigation, Methodology, Validation, Writing - original draft.

Departamento de Construção Civil | Universidade Federal do Paraná | Av. Coronel Francisco Heráclito dos Santos, 100, Jardim das Américas | Curitiba - PR - Brasil | CEP 82590-300 | Tel.: (46) 98822-6287 | E-mail: priscila-trentin@hotmail.com

#### **Caroline Angulski da Luz**

Formal analysis, Resources, Supervision, Validation, Writing - review & editing.

Departamento Acadêmico de Construção Civil | Universidade Tecnológica Federal do Paraná | Via do Conhecimento, s/n, KM 01, Fraron | Pato Branco - PR - Brasil | CEP 85503-390 | Tel.: (46) 99121-2222 | E-mail: angulski@hotmail.com

#### **Ronaldo Alves de Medeiros-Junior**

Formal analysis, Funding acquisition, Supervision, Validation, Writing - review & editing.

Departamento de Construção Civil | Universidade Federal do Paraná | Tel.: (41) 99215-4031 | E-mail: medeirosjunior.ufpr@gmail.com

Editor: **Marcelo Henrique Farias de Medeiros**

Editoras de seção: **Ercília Hitomi Hirota e Juliana Parise Baldauf**

### ***Ambiente Construído***

Revista da Associação Nacional de Tecnologia do Ambiente Construído

Av. Osvaldo Aranha, 99 - 3º andar, Centro

Porto Alegre - RS - Brasil

CEP 90035-190

Telefone: +55 (51) 3308-4084

[www.seer.ufrgs.br/ambienteconstruido](http://www.seer.ufrgs.br/ambienteconstruido)

[www.scielo.br/ac](http://www.scielo.br/ac)

E-mail: [ambienteconstruido@ufrgs.br](mailto:ambienteconstruido@ufrgs.br)



This is an open-access article distributed under the terms of the Creative Commons Attribution License.